

Control of femtosecond multi-filamentation in glass by designable patterned optical fields

Ping-Ping Li,¹ Meng-Qiang Cai,¹ Jia-Qi Lü,¹ Dan Wang,¹ Gui-Geng Liu,¹ Sheng-Xia Qian,¹ Yongnan Li,¹ Chenghou Tu,^{1,a} and Hui-Tian Wang^{1,2,3,b}

¹MOE Key Laboratory of Weak Light Nonlinear Photonics and School of Physics, Nankai University, Tianjin 300071, China

²National Laboratory of Solid State Microstructures and School of Physics, Nanjing University, Nanjing 210093, China

³Collaborative Innovation Center of Advanced Microstructures, Nanjing University, Nanjing 210093, China

(Received 20 July 2016; accepted 20 November 2016; published online 5 December 2016)

We present a scheme for realizing femtosecond multi-filamentation with designable quantity and locations of filaments, based on the control of multi-focal spots formed by patterned optical fields (POFs) composed of multiple individual optical fields (IOFs). A computer-controlled spatial light modulator is used to engineer the POFs. In particular, we introduce a blazed phase grating in any IOF, which increases a degree of freedom, making the engineering of multi-focal spots becomes more flexible. We achieve experimentally the aim controlling femtosecond multi-filamentation in a K9 glass. Our scheme has great flexibility and convenience in controlling the multi-filamentation in quantity and locations of filaments and strength of interaction between filaments. © 2016 Author(s). All article content, except where otherwise noted, is licensed under a Creative Commons Attribution (CC BY) license (<http://creativecommons.org/licenses/by/4.0/>) [<http://dx.doi.org/10.1063/1.4971427>]

I. INTRODUCTION

Light filamentation produced by the femtosecond (fs) laser has aroused great interest since it was discovered for the first time in 1995.¹ When the laser power is higher than a certain critical value, the multi-filamentation can be observed experimentally due to the fluctuation in intensity or the perturbation in index.^{2–5} Many efforts have focused on the control of multiple filaments, such as by using the deformable mirror,⁶ the axicon,^{7–10} the phase plate,^{11–14} the pinhole,¹⁵ the diffractive elements,^{16,17} the mesh,^{18,19} the astigmatic focusing,^{20,21} the beam size,^{22–24} the ellipticity,^{25–28} the cylindrical lens,²⁹ the microlens array,³⁰ and the hybridly polarized vector fields.³¹

In this article, we present a scheme for controlling the fs multi-filamentation with the engineerable quantity and locations in a K9 glass (it is almost the same as BK-7 glass, so for all parameters used for K9 here, we can adopt those for BK-7^{32,33}). We used a computer-controlled spatial light modulator (SLM) to manipulate the patterned optical fields (POFs) composed of multiple individual optical fields (IOFs) and then to control the multi-focal spots in the focal plane. We demonstrate experimentally the realization of the designable, engineerable, and stable multi-filamentation in the K9 glass.

II. EXPERIMENT

The experimental configuration is shown in Fig. 1. The used light source was a fs Ti-sapphire regenerative amplifier (Coherent Inc.) operating at a central wavelength of 800 nm, with a pulse duration of 125 fs and a repetition rate of 1 kHz, which delivers a fundamental Gaussian mode. An achromatic half-wave plate (HWP) and a Glan-Taylor prism (GTP) are used to control the energy and

^atuchenghou@nankai.edu.cn

^bhtwang@nju.edu.cn

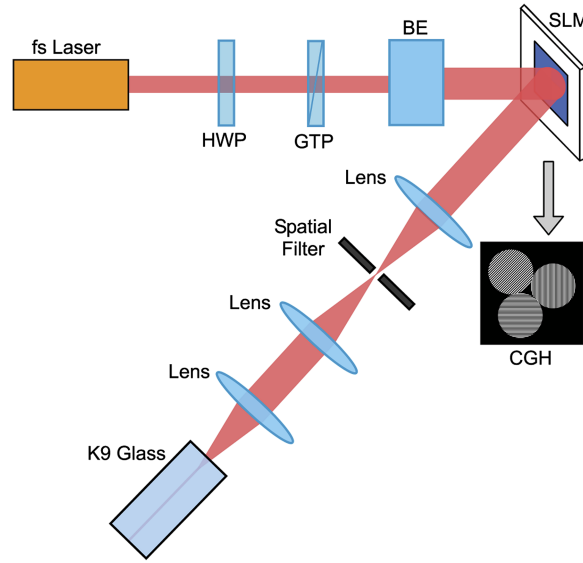


FIG. 1. Experimental configuration for producing the fs multi-filamentation. HWP—half-wave plate, GTP—Glan-Taylor prism, BE—Beam expander, CGH—computer-generated hologram, SLM—spatial light modulator.

the polarization direction of the laser incident into the K9 glass. After the fs laser beam is expanded by a beam expander (BE) composed of a pair of achromatic lenses, it is incident on the reflection-type SLM (with a dimension of 1920×1080 pixels and a size of $p \times p = 8 \times 8 \mu\text{m}^2$ per pixel). The computer-generated holograms (CGHs) displayed on the SLM are used to produce the POFs composed of multiple IOFs. Behind the SLM, another pair of achromatic lenses is used for the spatial filtering. A focusing achromatic lens with a focal length of 200 mm is used to increase the energy density inside the K9 glass (with a length of ~ 15 mm) and the focal plane is inside the K9 glass (with a distance of ~ 2 mm from the incident plane of the K9 glass). The produced multi-filaments are imaged by an achromatic lens with a focal length of 50 mm. The CCD camera is used to capture the images, for recording a frame of image is in 10 shots. The images we captured by the CCD camera were the end plane of the filaments instead of the exit plane of the glass sample. After the end plane of the filaments, the filaments will exhibit rapid divergence, so the local intensity becomes very low, which results in the very low nonlinear effect. Therefore, the images captured on the CCD camera will have only a little distortion, because the propagation of the divergent filaments is near linear behind the end plane of the filaments. The imaging system is an achromatic lens with a focal length of 50 mm. The very low nonlinearity can only give rise to a little change in size of filament, while cannot influence on the location of the filament.

The computer-controlled SLM is used to generate the demanded POFs. The reflection function of the CGH loaded on the SLM is written as

$$t(x, y) = \frac{1}{2} + \frac{1}{2}\gamma \cos [2\pi f_x x + \delta(x, y)]. \quad (1)$$

The demanded information, which is included in $\delta(x, y)$, is carried by the carrying-frequency grating $\cos(2\pi f_x x)$ along the x direction, with a grating period of $\Lambda = 10p$ (with a corresponding spatial frequency $f_x = 1/\Lambda$). $\delta(x, y)$ has the following form

$$\delta(x, y) = \sum_{j=1}^n \text{circ} \left(\frac{|\mathbf{r} - \mathbf{r}_{0j}|}{R_0} \right) \mathbf{G}_j \cdot \mathbf{r} \quad (2)$$

with

$$\text{circ}(r/R_0) = \begin{cases} 1 & r \leq R_0 \\ 0 & \text{otherwise} \end{cases} \quad (3)$$

where $\mathbf{G}_j = (2\pi/\Lambda_j)\hat{\mathbf{k}}_j$, $\hat{\mathbf{k}}_j = \cos \phi_j \hat{\mathbf{x}} + \sin \phi_j \hat{\mathbf{y}}$, $\mathbf{r} = x\hat{\mathbf{x}} + y\hat{\mathbf{y}}$, $\hat{\mathbf{x}}$ and $\hat{\mathbf{y}}$ are the unit vectors in the x and y directions, and ϕ_j is an angle formed with the x direction, respectively.

An uniformly x -polarized optical field is incident on the SLM with a reflection function given in Eq. (1), to be diffracted into many orders. Only its +1st order is chosen as the input field as follows

$$E^{in}(x, y) = E_0 \sum_{j=1}^n \text{circ} \left(\frac{|\mathbf{r} - \mathbf{r}_{0j}|}{R_0} \right) e^{i \frac{2\pi}{\Lambda_j} (x \cos \phi_j + y \sin \phi_j)} \quad (4)$$

After such an input POF field composed of n IOFs is focused, it is incident into the K9 glass to produce the multi-filamentation. Each IOF is a circular top-hat field with the same radius of R_0 and the same amplitude of E_0 . The location of the j th IOF is defined by the coordinate of its center, as $\mathbf{r}_{0j} = (r_{0j}, \phi_{0j})$. In particular, one should be pointed out that each IOF carries a blazed long-period phase grating \mathbf{G}_j . The j th IOF has a grating period of Λ_j and an orientation (its grating vector $\hat{\mathbf{k}}_j$ has an orientation angle of ϕ_j with respect to the $+x$ direction). The focused input POF will include n focal spots from the n IOFs. Λ_j and ϕ_j of the j th IOF are used to engineering the arrangement of the n focal spots, and to achieve the engineering of the fs multi-filamentation in the nonlinear medium (K9 glass). The period Λ_j can be defined as $\Lambda_j = L_j p$, where L_j indicates the number of pixels within one period.

After focusing, the j th IOF in the input plane (x, y) or (r, ϕ) is focused into a focal spot in the focal plane (ρ, φ) , which is located at (ρ_j, φ_j) . We can calculate the distance ρ_j of the focal spot P_j from the field center ($\rho = 0$) by the formula $\tan \theta_j = \rho_j / f$, where f is the focal length of the focusing lens. Under the paraxial condition, the focal spot of the j th IOF is located at $(\rho_j, \varphi_j) = (f\lambda / \Lambda_j, \phi_j)$ in the focal plane (ρ, φ) . The diffraction angle (θ_j), which is an angle formed by the propagation direction z , is determined by $\sin \theta_j = \lambda / \Lambda_j$. So the distance of the focal spot from the center ($\rho = 0$) can be controlled by changing the period Λ_j of the phase grating in the j th IOF for a given f , while the orientation of the focal spot can be changed by the orientation angle ϕ_j .

We first generate a POF composed of three closely arranged IOFs with the same radius of $R_0 = 1872 \mu\text{m}$. With its focal field recorded by the CCD camera, as shown in Fig. 2(a), we measured the distance between focal spots 1 and 2 is $d \sim 328.2 \mu\text{m}$, and then estimated to be $\rho_1 = d / 2 \cos 30^\circ \sim 189.5 \mu\text{m}$. We also calculated the theoretical value of ρ_1 to be $\rho_1 = f\lambda / \Lambda_1 = 200 \mu\text{m}$ (where $f = 200 \text{ mm}$, $\lambda = 800 \text{ nm}$ and $\Lambda_1 = 100p = 800 \mu\text{m}$). When such a focused field is incident into the K9 glass, three filaments are produced and its pattern is also recorded, as shown in Fig. 2(b). We measured the distance between the corresponding filaments 1 and 2 to be $\sim 317.8 \mu\text{m}$ (correspondingly, the distance of the filament 1 or 2 to the center is $\rho'_1 \sim 183.5 \mu\text{m}$). Since $\rho'_1 \approx \rho_1$, the filaments are produced in the vicinity of focal field. The filaments 1 and 2 had the size of ~ 53.0 and $\sim 61.0 \mu\text{m}$ in the short dimension.

We now explore the engineering of quantity of multi-filaments. In the following, n and m are used to define the quantity of the grating units (or focal spots) on the CGH (in the focal plane) and of the filaments produced in the K9 glass, respectively. Figures 3(a)–(c) show the patterned CGH loaded on the computer-controlled SLM, which are used to generate the POFs composed of three ($n = 3$), four ($n = 4$) and five ($n = 5$) IOFs, respectively. In Fig. 3(a) the three closely arranged IOFs are located at $(r_{0j}, \phi_{0j}) = (270p, 2j\pi/3)$ ($j = 0, 1, 2$), in Fig. 3(b) the four closely arranged IOFs are

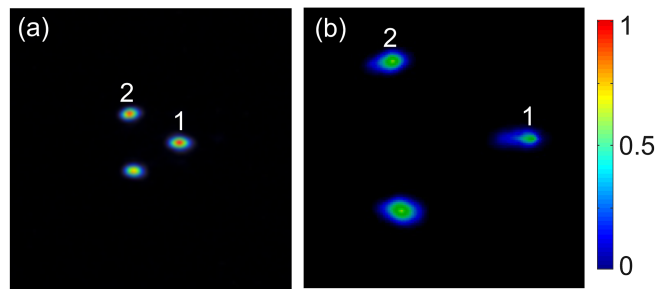


FIG. 2. The patterns of the focal spots and the filaments produced by the POF composed of three ($n = 3$) closely arranged IOFs. (a) The focused field pattern with a size of $1835 \times 1835 \mu\text{m}^2$. (b) The corresponding intensity pattern of filamentation with a size of $611.7 \times 611.7 \mu\text{m}^2$.

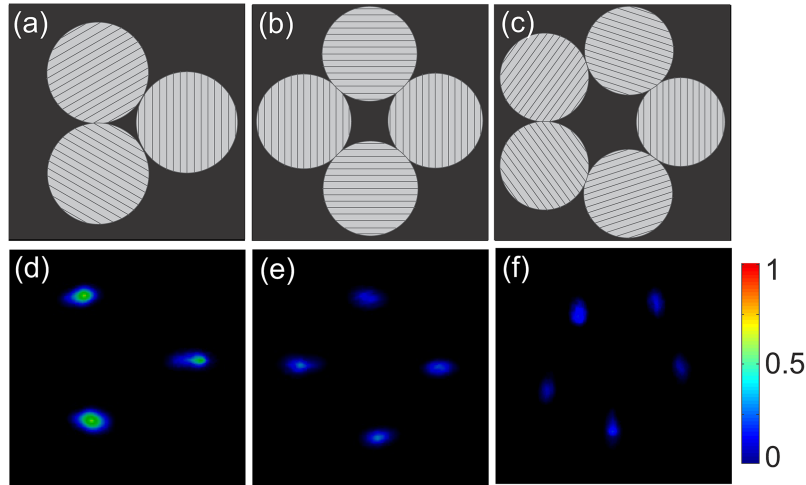


FIG. 3. The phase gratings of the input POFs and the patterns of the filaments produced by them. (a)–(c) The phase gratings loaded on the SLM, with $n = 3, 4, 5$. (d)–(f) The corresponding patterns of the produced filaments, with $n = 3, 4, 5$. Any photo had a size of $8640 \times 8640 \mu\text{m}^2$ (1080×1080 pixels) in (a)–(c). Any photo had a size of $611.7 \times 611.7 \mu\text{m}^2$ in (d)–(f).

located at $(r_{0j}, \phi_{0j}) = (310p, 2j\pi/4)$ ($j = 0, 1, 2, 3$), and in Fig. 3(c) the five closely arranged IOFs are located at $(r_{0j}, \phi_{0j}) = (335p, 2j\pi/5)$ ($j = 0, 1, 2, 3, 4$), respectively. One should be pointed out that the orientation angle of the phase grating in any IOF is $\phi_j = \phi_{0j}$ in Figs. 3(a)–(c), implying that any phase grating is oriented toward the origin. Figures 3(d)–(f) illustrate the spatial distribution of the filaments produced by the focused POFs shown in Figs. 3(a)–(c), respectively. Clearly, the quantity of the produced filaments are in good agreement with that of the IOFs $m = n$. The total energy per the single pulse incident into the K9 glass is $\varepsilon = 10.75, 10.75$ and $14.40 \mu\text{J}$, for the three cases of $n = m = 3$ in Fig. 3(a) and (d), $n = m = 4$ in Fig. 3(b) and (e), and $n = m = 5$ in Fig. 3(c) and (f), respectively. Correspondingly, the pulse peak power P for producing the single filament is estimated by $P = (\varepsilon/n)/\tau$ to be $28.7, 21.5$ and 23.0 MW, for the three cases, which are $15.6P_C, 11.7P_C$ and $12.5P_C$ (we estimated the critical power of self-focusing for the K9 glass to be $P_C = \alpha\lambda^2/8\pi n_0 n_2 \sim 1.84$ MW, by using $\alpha = 3.77, \lambda = 800$ nm, $n_0 = 1.51$ and $n_2 = 3.45 \times 10^{-20} \text{ m}^2/\text{W}^{32,33}$), respectively. We should pointed out that the input power of the IOF is not the power contained in a single filament. However, the filament contains a fixed amount of power, roughly equal to P_C (the critical power of self-focusing for the nonlinear medium).^{1,34} The filaments had a size of $\sim 52.0 \mu\text{m}$ in the short dimension.

We now explore the whole engineering of the multi-filamentation, including the whole rotation as shown in Fig. 4 and the interval between the filaments as shown in Fig. 5. We choose the POFs composed of three closely arranged IOFs as examples, under the pulse peak power of $P = 15.6P_C = 28.7$ MW. Figure 4(a) shows the intensity pattern of filamentation, which is produced by the focused POF composed of three closely arranged IOFs, with the same radius of $R_0 = 234p = 1872 \mu\text{m}$ and the same grating period $\Lambda_{1,2,3} = Lp = 50p$ ($L = 50$) = $400 \mu\text{m}$. The centers of three IOFs are located at $(r_{0j}, \phi_{0j}) = (270p, 2j\pi/3)$ ($j = 0, 1, 2$) and the orientation angles of the three grating are $\phi_j = \phi_{0j}$ ($j = 0, 1, 2$) (implying that the three gratings are orientated toward the origin). Figures 4(b)–(h) show a series of the intensity patterns of filamentation, produced by a series of the focused POFs, which are counterclockwise rotated by a step of $\pi/12$ with respect to the POF used in Fig. 4(a) in turn, as schematically shown in the inset in the right. The filaments had a size of $\sim 56.0 \mu\text{m}$ in the short dimension. Clearly, the intensity patterns of the produced filaments are also rotated by the same angle synchronously. So it is neatly to change the locations of filaments by rotating the grating units of the CGH loaded on the SLM. For the control on the interval between the filaments, the arrangement of the used POF is similar to that used in Fig. 4(a), the phase gratings of all the three IOFs are still oriented toward the origin while all the grating periods are changed synchronously. As shown in Figs. 5(a)–(l), the intervals between two neighbor filaments decrease as the grating periods $\Lambda_{1,2,3} = Lp$ increase, because the larger grating period in the IOF makes the focal spot has the smaller deflection

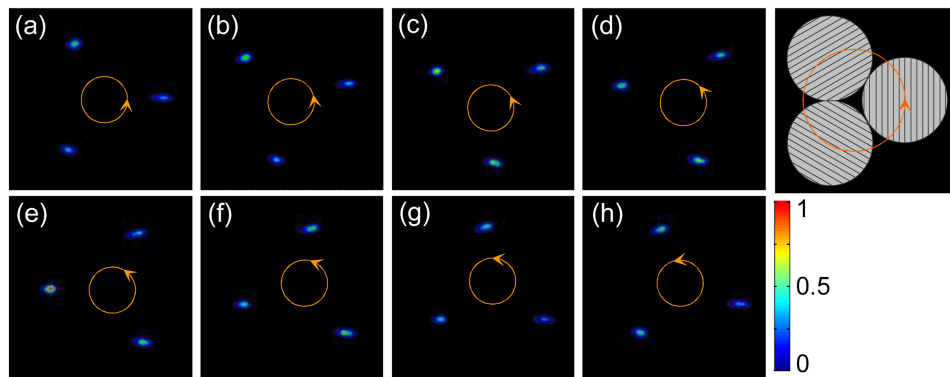


FIG. 4. The intensity patterns of the filaments produced by a series of the POFs composed of the three closely arranged IOFs, under the pulse peak power of $P = 15.3P_C = 28.2$ MW. In (a)-(h), the POFs are in turn rotated by a step of $\pi/12$. Any photo had a size of $1138 \times 1138 \mu\text{m}^2$.

angle. The filaments had a size of $\sim 66.0 \mu\text{m}$ in the short dimension. In Fig. 6, when the phase periods $\Lambda_{1,2,3} = Lp$ are changed from $L = 40$ to $L = 250$ pixels, the interval between the two neighbor filaments decreases from $d = 824$ to $132 \mu\text{m}$ (experimental values from Fig. 5) and from $d = 867$ to $138 \mu\text{m}$ (theoretical results). Clearly, the experimental results are in good agreement with the theoretical ones.

We now explore the control on a single filament, as shown in Fig. 7, under the pulse peak power of $P = 15.6P_C = 28.7$ MW. In this case, any POF is composed of three closely arranged IOFs. The centers of the three IOFs with the same radius of $R_0 = 234p$ are always located at $(r_{0j}, \phi_{0j}) = (270p, 2j\pi/3)$, where $j = 0, 1, 2$. The phase gratings in the three IOFs are always oriented toward the origin. In particular, the phase gratings of the 1st and 3rd IOFs located at $(r_{01}, \phi_{01}) = (270p, 0)$

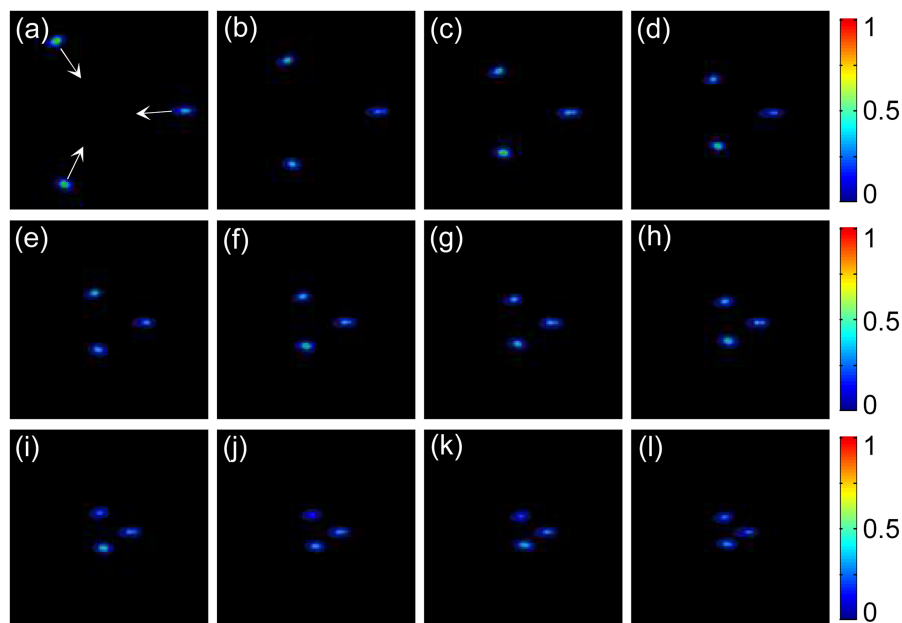


FIG. 5. The intensity patterns of multi-filamentation produced by a series of the POFs composed of three closely arranged IOFs under $P = 15.3P_C = 28.2$ MW, with different grating period. (a)-(l) correspond to $L = 40, 55, 70, 85, 100, 115, 130, 145, 160, 175, 190,$ and 205 pixels, respectively. Any photo had a size of $1138 \times 1138 \mu\text{m}^2$. Three arrows in (a) show the moving directions of the filaments with the grating period.

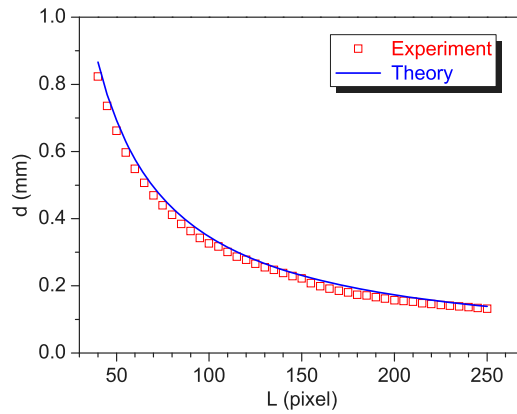


FIG. 6. Dependence of the interval between the two neighbor filaments among the three filaments on the grating period of the IOF. The opened squares are the measured intervals (from Fig. 5) and the solid line shows the calculated intervals between the two neighbor focal spots in the focal plane.

and $(r_{03}, \phi_{03}) = (270p, 4\pi/3)$ always keep the grating period of $\Lambda_1 = \Lambda_3 = 50p$. In contrast, the grating period Λ_2 of the 2nd IOF is changed from $L_2 = 50$ to $L_2 = 500$, and then further from $L_2 = -500$ to $L_2 = -100$ (the “-” sign indicates that the orientation of the blazed grating of the 2nd IOF is inverted). Clearly, the focal spots of the 1st and 3rd IOFs are fixed, while the focal spot of the 2nd IOF will move along the bisector of the focal spots of the 1st and 3rd IOFs because its grating period Λ_2 changes. From a series of the intensity patterns of the multi-filaments shown in

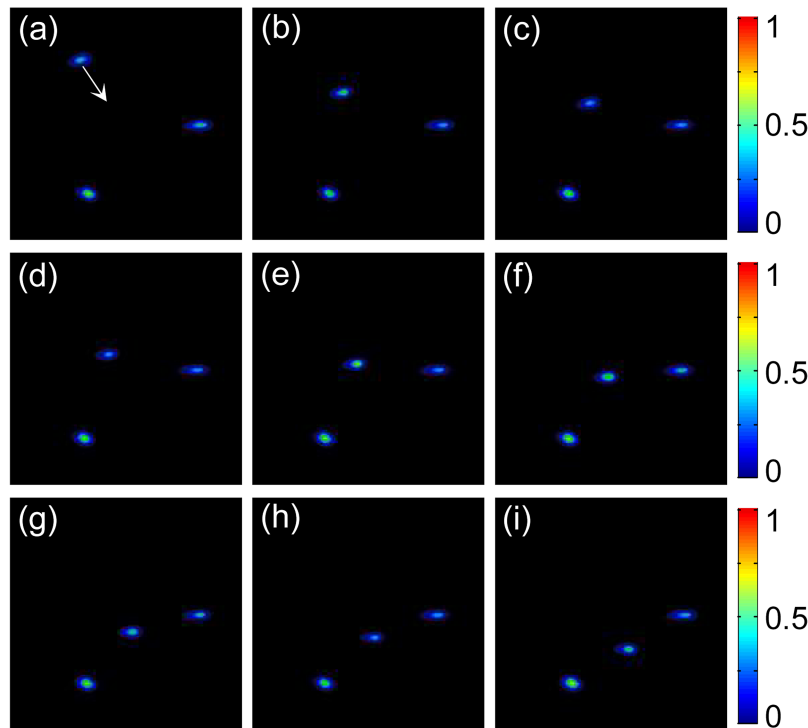


FIG. 7. The intensity patterns of filamentation produced by a series of the POFs composed of three closely arranged IOFs, with their centers always located at $(r_{01}, \phi_{01}) = (270p, 0)$, $(r_{02}, \phi_{02}) = (270p, 2\pi/3)$, and $(r_{03}, \phi_{03}) = (270p, 4\pi/3)$. The periods and orientations of the gratings in the 1st and 3rd IOFs are fixed. The grating period of the 2nd IOF is changed, with a series of values of $\Lambda_2 = L_2p$, where $L_2 = 50$ (a), $L_2 = 100$ (b), $L_2 = 150$ (c), $L_2 = 200$ (d), $L_2 = 500$ (e), $L_2 = -500$ (f), $L_2 = -200$ (g), $L_2 = -150$ (h), $L_2 = -100$ (i). Any photo had a size of $1138 \times 1138 \mu\text{m}^2$. Arrow in (a) shows the moving direction of the filament with the grating period Λ_2 of the 2nd IOF.

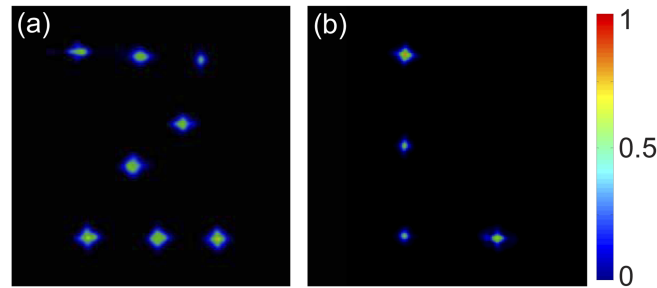


FIG. 8. The patterned filaments produced by the two special POFs. Any photo has a size of $1844 \times 1844 \mu\text{m}^2$.

Fig. 7, in any photo the two filaments are always stationary, while another filament moves from the top left corner to the bottom right corner along the bisector of the two stationary filaments as shown in Figs. 7(a)–(i). In addition, we also produce two patterned multi-filaments, as shown in Fig. 8. Multi-filaments exhibit the shapes of letters “Z” and “L”, as shown in Figs. 8(a) and (b), respectively.

III. DISCUSSION

We show two examples of the top views of propagation process of light in the glass in Fig. 9. Clearly, it is indubitable that the light propagates indeed in the self-trapping channels in the glass, in Figs. 9(a) and (b), there have two and three filaments with a length of ~ 12 mm, respectively. If there has no nonlinear effect, the light in glass will be divergent or diffuse. The higher-order nonlinear effect plays an important role in filamentation, because it can balance the self-diffraction to form the filaments.

As another proof, the filamentation is always accompanied by supercontinuum generation. Figure 10 shows the color conical supercontinuum patterns captured on a white screen placed behind the glass. Since if there has no filamentation, it is very difficult to generate the supercontinuum, which is an indication of the filamentation. We also measure the supercontinuum spectra generated by the POF composed of three IOFs ($n = m = 3$) with different grating period $\Lambda = Lp$, as shown in Fig. 11. It can be found that as the grating period Λ (L) increases, the intensity of the supercontinuum exhibits a trend of slightly stronger, and the supercontinuum spectra have two peaks located at the shorter wavelength of ~ 600 nm and the longer wavelength of ~ 734 nm, respectively. As the period Λ (L) increases, the shorter wavelength peak exhibits a blue shift from 618 nm for $L = 250$ pixels to 590 nm for $L = 850$ pixels and its intensity increases, while the longer wavelength peak has no almost shift and its intensity increases quickly. As the period increases, as shown in Fig. 5, the filaments are close to each other until partially overlap, resulting in the stronger interaction between the filaments and the enhancement of supercontinuum generation.

At last, the precision of the aim in terms of angle and distance depends dominantly on the size of each pixel of the spatial light modulator. The smaller size of pixel will get the higher precision. Since each pixel had a size of $p \times p = 8 \times 8 \mu\text{m}^2$, the maximum angular uncertainty and the

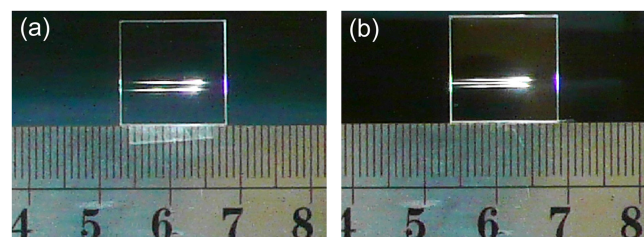


FIG. 9. The top views of the light filaments propagating inside the glass. (a) The case of $n = m = 2$ and $L = 40$ pixels and (b) the case of $n = m = 3$ and $L = 40$ pixels.

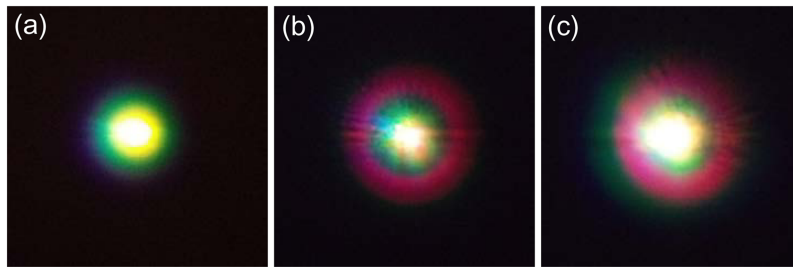


FIG. 10. The supercontinuum patterns captured on a white screen placed behind the glass for three POFs with the same $n = m = 3$ in the K9 glass, but different periods $L = 40$ pixels (a), $L = 250$ pixels (b), and $L = 900$ pixels (c).

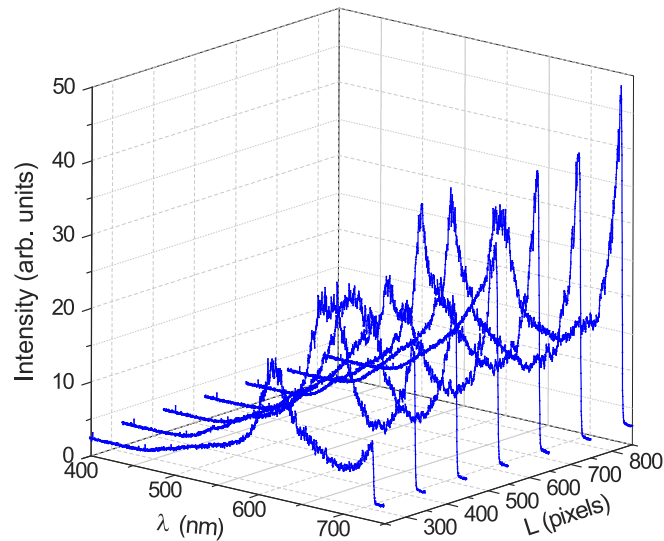


FIG. 11. The measured supercontinuum spectra produced by the POFs composed of three IOFs with $n = m = 3$ in the K9 glass, for different periods of $\Lambda = Lp$ ($L = 250$ to 850).

maximum distance uncertainty are lower than 0.5 seconds and $0.6 \mu\text{m}$ in our experimental conditions, respectively.

IV. CONCLUSION

We have demonstrated the multi-filamentation produced by the focused POFs composed of multiple IOFs in the solid glass. In particular, each IOF includes a blazed phase grating, its period and orientation, as degrees of freedom, can flexibly engineer the location of focal spot of the IOF. The quantity of IOFs consisting the POF can determine the quantity of focal spots. The computer-controlled SLM can be used to achieve our aim. Due to the engineerable patterns of the multi-focal spots, the multi-filamentation produced by the fs POF composed of multiple IOFs can be flexibly engineered. Although our idea has proved in the solid glass, our scheme should have some reference significance for producing the engineerable multi-filamentation in air. Inasmuch as our scheme is able to easily control the intervals between the filaments by setting the locations of individual optical fields forming the patterned optical field, which allows us to tune the strength of interaction between the filaments. When the filaments are close to each other, the interaction becomes stronger. In this article, however, we do not deeply investigate the interaction between the filaments. Due to the flexible controllability, our scheme should be a promising one for developing the potential applications of filaments. For example, the laser control triggering

lightning maybe become more convenient and flexible in the operability of quantity and locations of filaments.

ACKNOWLEDGMENTS

We acknowledge the support by National Natural Science Foundation of China (11534006 and 11374166), Natural Science Foundation of Tianjin (16JC2DJC31300), National scientific instrument and equipment development project (2012YQ17004), and Collaborative Innovation Center of Extreme Optics.

- ¹ A. Braun, G. Korn, X. Liu, D. Du, J. Squier, and G. Mourou, "Self-channeling of high-peak-power femtosecond laser pulses in air," *Opt. Lett.* **20**, 73–75 (1995).
- ² G. Paunescu, G. Spindler, W. Riede, H. Schröder, and A. Giesen, "Multifilamentation of femtosecond laser pulses induced by small-scale air turbulence," *Appl. Phys. B* **96**, 175–183 (2009).
- ³ G. Spindler and G. Paunescu, "Multifilamentation of femtosecond laser pulses propagating in turbulent air near the ground," *Appl. Phys. B* **96**, 185–191 (2009).
- ⁴ S. L. Chin, A. Talebpour, J. Yang, S. Petit, V. P. Kandidov, O. G. Kosareva, and M. P. Tamarov, "Filamentation of femtosecond laser pulses in turbulent air," *Appl. Phys. B* **74**, 67–76 (2002).
- ⁵ T. T. Xi, X. Lu, and J. Zhang, "Interaction of light filaments generated by femtosecond laser pulses in air," *Phys. Rev. Lett.* **96**, 025003 (2006).
- ⁶ C. P. Hauri, J. Gautier, A. Trisorio, E. Papalazarou, and P. Zeitoun, "Two-dimensional organization of a large number of stationary optical filaments by adaptive wave front control," *Appl. Phys. B* **90**, 391–394 (2008).
- ⁷ B. Zhou, S. Akturk, B. Prade, Y. B. André, A. Houard, Y. Liu, M. Franco, C. D'Amico, E. Salmon, Z. Q. Hao, N. Lascoux, and A. Mysyrowicz, "Revival of femtosecond laser plasma filaments in air by a nanosecond laser," *Opt. Express* **17**, 11450–11456 (2009).
- ⁸ S. Akturk, B. Zhou, M. Franco, A. Couairon, and A. Mysyrowicz, "Generation of long plasma channels in air by focusing ultrashort laser pulses with an axicon," *Opt. Commun* **282**, 129–134 (2009).
- ⁹ P. Polynkin, A. Kolesik, A. Roberts, D. Faccio, P. Di Trapani, and J. Moloney, "Generation of extended plasma channels in air using femtosecond Bessel beams," *Opt. Express* **16**, 15733–15740 (2008).
- ¹⁰ X. D. Sun, H. Gao, B. Zeng, S. Q. Xu, W. W. Liu, Y. Cheng, Z. Z. Xu, and G. G. Mu, "Multiple filamentation generated by focusing femtosecond laser with axicon," *Opt. Lett.* **37**, 857–859 (2012).
- ¹¹ T. Pfeifer, L. Gallmann, M. J. Abel, D. M. Neumark, and S. R. Leone, "Circular phase mask for control and stabilization of single optical filaments," *Opt. Lett.* **31**, 2326–2328 (2006).
- ¹² P. Rohwetter, M. Queißer, K. Stelmaszczyk, M. Fechner, and L. Wöste, "Laser multiple filamentation control in air using a smooth phase mask," *Phys. Rev. A* **77**, 013812 (2008).
- ¹³ Y. X. Fu, H. Xiong, H. Xu, J. P. Yao, B. Zeng, W. Chu, Y. Cheng, Z. Z. Xu, W. W. Liu, and S. L. Chin, "Generation of extended filaments of femtosecond pulses in air by use of a single-step phase plate," *Opt. Lett.* **34**, 3752–3754 (2009).
- ¹⁴ H. Gao, W. Chu, G. Yu, B. Zeng, J. Zhao, Z. Wang, W. W. Liu, Y. Cheng, and Z. Z. Xu, "Femtosecond laser filament array generated with step phase plate in air," *Opt. Express* **21**, 4612–4621 (2013).
- ¹⁵ Z. Q. Hao, J. Zhang, T. T. Xi, X. H. Yuan, Z. Y. Zheng, X. Lu, M. Y. Yu, Y. T. Li, Z. H. Wang, W. Zhao, and Z. Y. Wei, "Optimization of multiple filamentation of femtosecond laser pulses in air using a pinhole," *Opt. Express* **15**, 16102–16109 (2007).
- ¹⁶ G. Méchain, A. Couairon, M. Franco, B. Prade, and A. Mysyrowicz, "Organizing multiple femtosecond filaments in air," *Phys. Rev. Lett.* **93**, 035003 (2004).
- ¹⁷ L. Guyon, K. M. Hajek, F. Courvoisier, V. Boutou, R. Nuter, A. Vincotte, S. Champeaux, L. Bergé, and J. P. Wolf, "Control of lasing filament arrays in nonlinear liquid media," *Appl. Phys. B* **90**, 383–390 (2008).
- ¹⁸ J. Liu, H. Schroeder, S. L. Chin, R. Li, and Z. Xu, "Ultrafast control of multiple filamentation by ultrafast laser pulses," *Appl. Phys. Lett.* **87**, 161105 (2005).
- ¹⁹ H. Schroeder, J. Liu, and S. L. Chin, "From random to controlled small-scale filamentation in water," *Opt. Express* **12**, 4768–4774 (2004).
- ²⁰ G. Fibich, S. Eisenmann, B. Ilan, and A. Zigler, "Control of multiple filamentation in air," *Opt. Lett.* **29**, 1772–1774 (2004).
- ²¹ Y. Fu, H. Gao, W. Chu, J. Ni, H. Xiong, H. Xu, J. Yao, B. Zeng, W. Liu, Y. Cheng, Z. Xu, and S. L. Chin, "Control of filament branching in air by astigmatically focused femtosecond laser pulses," *Appl. Phys. B* **103**, 435–439 (2011).
- ²² Q. Luo, S. A. Hosseini, W. Liu, J. F. Gravel, O. G. Kosareva, N. A. Panov, N. Aközbek, V. P. Kandidov, G. Roy, and S. L. Chin, "Effect of beam diameter on the propagation of intense femtosecond laser pulses," *Appl. Phys. B* **80**, 35–38 (2004).
- ²³ V. P. Kandidov, N. Aközbek, M. Scalora, O. G. Kosareva, A. V. Nyakk, Q. Luo, S. A. Hosseini, and S. L. Chin, "Towards a control of multiple filamentation by spatial regularization of a high-power femtosecond laser pulse," *Appl. Phys. B* **80**, 267–275 (2005).
- ²⁴ O. G. Kosareva, N. A. Panov, N. Aközbek, V. P. Kandidov, Q. Luo, S. A. Hosseini, W. Liu, J. F. Gravel, G. Roy, and S. L. Chin, "Controlling a bunch of multiple filaments by means of a beam diameter," *Appl. Phys. B* **82**, 111–122 (2006).
- ²⁵ D. Majus, V. Jukna, G. Tamošauskas, G. Valiulis, and A. Dubietis, "Three-dimensional mapping of multiple filament arrays," *Phys. Rev. A* **81**, 043811 (2010).
- ²⁶ A. Dubietis, G. Tamošauskas, G. Fibich, and B. Ilan, "Multiple filamentation induced by input-beam ellipticity," *Opt. Lett.* **29**, 1126–1128 (2004).
- ²⁷ T. D. Grow and A. L. Gaeta, "Dependence of multiple filamentation on beam ellipticity," *Opt. Express* **13**, 4594–4599 (2005).

- ²⁸ D. Majus, V. Jukna, G. Valiulis, and A. Dubietis, "Generation of periodic filament arrays by self-focusing of highly elliptical ultrashort pulsed laser beams," *Phys. Rev. A* **79**, 033843 (2009).
- ²⁹ J. P. Bérubé, R. Vallée, M. Bernier, O. Kosareva, N. Panov, V. Kandidov, and S. L. Chin, "Self and forced periodic arrangement of multiple filaments in glass," *Opt. Express* **18**, 1801–1809 (2010).
- ³⁰ T. T. Xi, Z. J. Zhao, and Z. Q. Hao, "Femtosecond laser filamentation with a microlens array in air," *J. Opt. Soc. Am. B* **32**, 163–166 (2015).
- ³¹ S. M. Li, Y. N. Li, X. L. Wang, L. J. Kong, K. Lou, C. H. Tu, Y. J. Tian, and H. T. Wang, "Taming the collapse of optical fields," *Sci. Rep.* **2**, 1007 (2012).
- ³² T. Y. Chang, "Fast self-induced refractive index changes in optical media: a survey," *Opt. Eng.* **20**, 220–232 (1981).
- ³³ D. Huang, M. Ulman, L. H. Acioli, H. A. Haus, and J. G. Fujimoto, "Self-focusing-induced saturable loss for laser mode locking," *Opt. Lett.* **17**, 511–513 (1992).
- ³⁴ A. Couairon and A. Mysyrowicz, "Femtosecond filamentation in transparent media," *Phys. Rep.* **441**, 47–189 (2007).